

Precipitation and its extremes in changed climates

T. Schneider and P. A. O’Gorman

California Institute of Technology, Pasadena, CA, USA

Abstract. While the specific humidity of the atmosphere is expected to increase as the climate warms, roughly consistent with constant relative humidity in a global mean, precipitation increases do not keep pace with specific humidity increases. To investigate systematically how precipitation changes with climate, we conducted a series of simulations with an idealized general circulation model in which we varied the optical thickness of the longwave absorber. In the simulations, global-mean precipitation increases approximately linearly with global-mean surface air temperature over a wide range of climates and asymptotically approaches a maximum in warm climates, with the maximum estimable from the surface energy budget. The large-scale (grid-scale) precipitation, which is particularly important in the extratropics, exhibits more complex behavior, with a maximum in a moderately warm climate and smaller values in colder and warmer climates. Changes in precipitation extremes likewise do not scale with specific humidity changes but exhibit more complex behavior, with a wide range in which they increase approximately linearly with global-mean surface air temperature at a fractional rate approximately equal to that of the mean precipitation and, for some extreme-value statistics, with a maximum or plateau in warm climates.

1. Introduction

According to the Clausius-Clapeyron relation, a small change δT in temperature T leads to a fractional change $\delta e_s/e_s$ in saturation vapor pressure e_s of

$$\frac{\delta e_s}{e_s} \approx \frac{L}{R_v T^2} \delta T, \quad (1)$$

where R_v is the gas constant of water vapor and L is the latent heat of vaporization. If one substitutes representative values for the present-day Earth climate, this implies that the fractional increase in saturation vapor pressure with temperature is about 6–7% K⁻¹ (e.g., *Trenberth et al.* [2003]). *Held and Soden* [2006] showed that in simulations of 21st-century climate change scenarios, the fractional increase in global-mean precipitable water (column-integrated specific humidity) with global-mean surface temperature is about 7.5% K⁻¹, similar to the fractional increase in saturation vapor pressure and roughly consistent with a constant effective relative humidity (a relative-humidity average weighted by the saturation vapor pressure, i.e., toward the lower troposphere). On the other hand, the fractional increase in global-mean precipitation and evaporation with global-mean surface temperature is about 2.2% K⁻¹—considerably less than the specific humidity increase.

Changes in evaporation and precipitation and in

near-surface saturation specific humidity and relative humidity are closely related. According to the bulk aerodynamic formula, evaporation E over oceans is related to the specific humidity q near the surface and the saturation specific humidity q_s^* at the surface by

$$E = \rho C_W \|\mathbf{v}\| (q_s^* - q), \quad (2)$$

where ρ is the density of near-surface air, \mathbf{v} is the near-surface wind, and C_W is a bulk transfer coefficient (e.g., *Peixoto and Oort* [1992]). Over oceans, the disequilibrium factor $q_s^* - q$ between the surface and near-surface air is usually dominated by the subsaturation of near-surface air, rather than by the temperature difference between the surface and near-surface air, so that it can be approximated as $q_s^* - q \approx (1 - \mathcal{H})q_s^*$, with near-surface relative humidity \mathcal{H} . If one further assumes that changes in evaporation with climate are dominated by changes in the disequilibrium factor $q_s^* - q$ and that its changes, in turn, are dominated by changes in near-surface saturation specific humidity and relative humidity, the fractional change $\delta E/E$ in evaporation E can be expressed as

$$\frac{\delta E}{E} = \frac{\delta q_s^*}{q_s^*} - \frac{\delta \mathcal{H}}{1 - \mathcal{H}}. \quad (3)$$

As discussed by *Held and Soden* [2000], the relation (3) together with the surface energy budget constrains

the changes in evaporation and near-surface relative humidity that are possible for a given change in radiative forcing and temperature. With a fractional change of $2.2\% \text{ K}^{-1}$ in evaporation and $6.5\% \text{ K}^{-1}$ in saturation vapor pressure, a global-mean surface temperature increase of 3 K leads to a global-mean increase in evaporation of $\delta E/E \approx 6.6\%$ and in saturation specific humidity at the surface of $\delta q_s^*/q_s^* \approx \delta e_s/e_s \approx 19.5\%$. To the extent that the relation (3) is adequate, it follows that the relative humidity term $\delta \mathcal{H}/(1-\mathcal{H})$ increases by about $(19.5 - 6.6)\% = 12.9\%$, or, with a typical near-surface relative humidity of 80% , the relative humidity increases by about 2.6 percentage points. The precise magnitude of relative humidity changes will depend on changes in surface winds and in the temperature difference between the surface and near-surface air. However, even if, for example, the influence of changes in the difference between surface and near-surface air on the disequilibrium factor $q_s^* - q$ is similar to the influence of changes in the near-surface relative humidity, the order of magnitude of the terms shows that changes in near-surface relative humidity will be small compared with changes in near-surface saturation specific humidity. This is especially the case if near-surface air is close to saturation so that the factor $1/(1-\mathcal{H})$ in (3) is large. Because most water vapor in the atmosphere is confined near the surface (the water vapor scale height is about 2 km), this implies that changes in precipitable water will be dominated by changes in near-surface saturation specific humidity.

It is also clear that fractional evaporation changes with surface temperature cannot be of a vastly different magnitude than the $2.2\% \text{ K}^{-1}$ quoted above, as would be necessary for significant relative humidity changes. For example, if an increase in the concentration of greenhouse gases would lead to a 3-K global-mean surface temperature increase in a statistically steady state, associated with a saturation specific humidity increase of about 19.5% , and would lead to a reduction in near-surface relative humidity from 80% to 70% , evaporation would have to increase by about 70% according to (3). But currently total evaporation at Earth’s surface amounts to a latent heat flux of about 80 W m^{-2} (Kiehl and Trenberth [1997]). A 70% increase would amount to an additional energy flux of 56 W m^{-2} that would have to be available to the surface, in the form of increased net irradiance or increased downward sensible heat fluxes, to balance the additional evaporation. But this is not possible given current estimates of the equilibrium climate sensitivity (of order 0.8 K surface warming per 1 W m^{-2} radiative forcing at the top of the atmosphere) and estimates of the additional energy flux available to the surface in a warmer climate, which is expected to be of the same order as but is not nec-

essarily equal to the radiative forcing at the top of the atmosphere that produced the warming. Notwithstanding uncertainties in quantitative details, the implication is that changes in near-surface relative humidity and in evaporation—and thus, in a statistically steady state, in precipitation—are strongly energetically constrained.

We recently investigated how the hydrologic cycle changes with climate in a much wider range of climates than those considered in typical global-warming simulations (O’Gorman and Schneider [2007b]). We simulated a wide range of climates with an idealized aqua-planet general circulation model (GCM) by systematically varying the optical thickness of an idealized long-wave absorber, which may be thought of as representing the combined effect of water vapor and well-mixed greenhouse gases. Other quantities such as the latent heat of vaporization, surface albedo, solar irradiance, and solar absorption in the atmosphere are kept fixed. The simulated climates have steady and zonally and hemispherically symmetric circulation statistics. They exhibit global-mean surface air temperatures between 260 K (pole-to-equator temperature contrast 70 K) and 316 K (pole-to-equator temperature contrast 24 K) and span climates from some resembling that of present-day Earth to equable climates and cold climates resembling those that may have occurred over Earth’s history. Here we summarize some results of our study. Section 2 and 3 summarize results on global-mean precipitation and large-scale precipitation (precipitation arising from large-scale condensation). These sections are a review of O’Gorman and Schneider [2007b]; more details and a model description can be found there. Section 4 presents results on precipitation extremes.

2. Global-mean precipitation

Figure 1 shows the global-mean precipitable water as a function of global-mean surface air temperature in the series of simulations. The precipitable water (solid line with circles) increases monotonically with surface air temperature, roughly consistent with a constant effective relative humidity (dashed line). The fractional rate of increase in precipitable water at the reference simulation (filled circle, a simulation with a climate close to that of present-day Earth) is $6.2\% \text{ K}^{-1}$, consistent with (1). The relative humidity in the free atmosphere does change over the range of simulations, but near the surface, where the bulk of the water vapor is confined, its changes are sufficiently small that assuming a constant effective relative humidity is a good approximation.

The increase in precipitation does not keep pace with the increase in precipitable water. Figure 2 shows the global-mean precipitation as a function of global-mean surface air temperature. Over a wide range of climates,

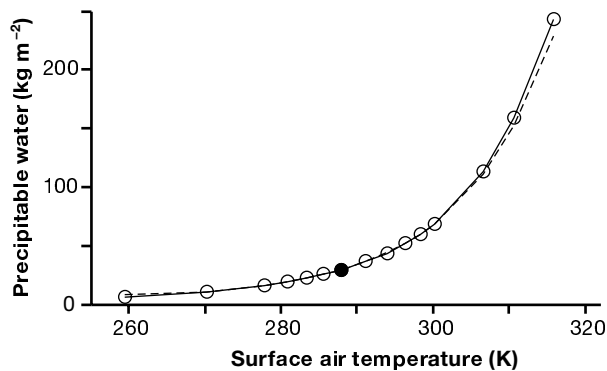


Figure 1. Global-mean precipitable water vs global-mean surface air temperature (solid line with circles). Here and in subsequent figures, the filled circle indicates a reference simulation with global-mean surface air temperature close to that of present-day Earth. The dashed line is the global and column average of the saturation specific humidity, excluding levels at the top of the model and rescaled by a constant relative-humidity factor of 0.67. (From *O’Gorman and Schneider* [2007b].)

the precipitation increases approximately linearly with surface air temperature. In warm climates, the precipitation asymptotically approaches a maximum value, which can be estimated from the surface energy budget. In warm climates, the dominant balance in the surface energy budget is between absorbed solar irradiance and the latent heat flux associated with evaporation; the relative importance of the net longwave radiative flux and of the sensible heat flux in the surface energy budget decreases as the climate warms. Because in a statistically steady state, precipitation is equal to evaporation, we obtain an approximate upper bound on precipitation,

$$P_{\max} \simeq (1 - \alpha)S/L, \quad (4)$$

if we set the latent heat flux $LE = LP$ at the surface equal to the absorbed solar irradiance $(1 - \alpha)S$, where α is the surface albedo and S is the solar irradiance at the surface (both are constant in our series of simulations). Figure 2 shows that this upper bound is a good estimate of the asymptotic maximum value of precipitation, though it is exceeded slightly in the warmest simulations because there is a net sensible heat flux from the atmosphere into the surface in those simulations. In general, the degree to which the bound (4) is attained depends on the sensible heat flux into or out of the surface and thus on boundary-layer dynamics.

Figure 2 also shows the precipitation change obtained if one assumes that changes in latent heat release within the atmosphere, and thus changes in evaporation and precipitation, are balanced by changes in the longwave radiative loss of the atmosphere (e.g., *Allen and Ingram*

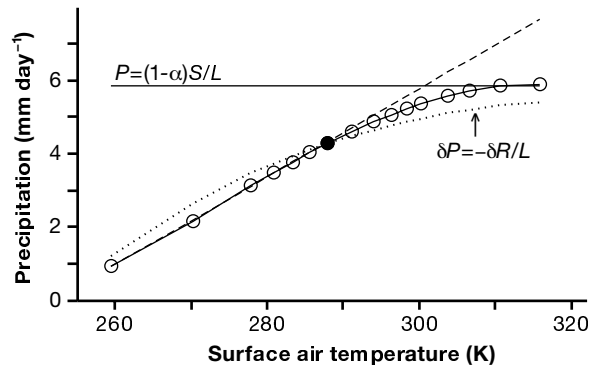


Figure 2. Global-mean precipitation vs global-mean surface air temperature (solid line with circles). The dashed line represents a linear increase of $2.8\% \text{ K}^{-1}$ relative to the reference simulation. The horizontal solid line is the approximate precipitation bound (4) corresponding to a balance of absorbed solar irradiance and evaporation at the surface. The dotted line shows the precipitation change (5) balanced by changes in the longwave radiative loss of the atmosphere, with a constant offset chosen such that there is agreement with the precipitation for the reference simulation. (From *O’Gorman and Schneider* [2007b].)

[2002]). The longwave radiative loss of the atmosphere is the difference between the outgoing longwave flux and the net upward longwave flux at the surface. Denoting the net upward longwave flux at the surface by R and using that, in our series of simulations, the latent heat of vaporization and the global-mean outgoing longwave radiation are constant, the precipitation change balanced by changes in longwave radiative loss is

$$\delta P = -\delta R/L. \quad (5)$$

Figure 2 shows that the precipitation change balanced by changes in longwave radiative loss is similar to the actual precipitation change, but the estimate (5) is not quantitatively accurate. Changes in sensible heat flux at the surface are not negligible. In particular, the estimate (5) does not account for the linear dependence of precipitation on surface air temperature over a wide range of the simulated climates. Moreover, even if the estimate (5) were more accurate, its use for estimating precipitation changes would be limited because the longwave flux at the surface depends on the surface air temperature and thus on the evaporation at the surface, making (5) an implicit relation.

We currently do not have a theory that accounts for the dependence of precipitation on surface air temperature. Radiative-convective equilibrium simulations with the same GCM as used in Fig. 2 give a similar dependence of precipitation on surface air temperature and suggest that energy constraints may account for it; see *O’Gorman and Schneider* [2007b].

3. Large-scale precipitation

Precipitation in GCMs can be decomposed into a component associated with parameterized convection and a component associated with large-scale (grid-scale) condensation. The latter component results from resolved motions. One may hope that it is less dependent on specifics of the convection parameterization than the convective component, but inasmuch as the resolved motions (particularly convection on the grid scale) depend on specifics of the convection parameterization, this may not be true. In our simulations, the large-scale component (“large-scale precipitation”) is largest in the extratropics, and the convective component dominates in lower latitudes.

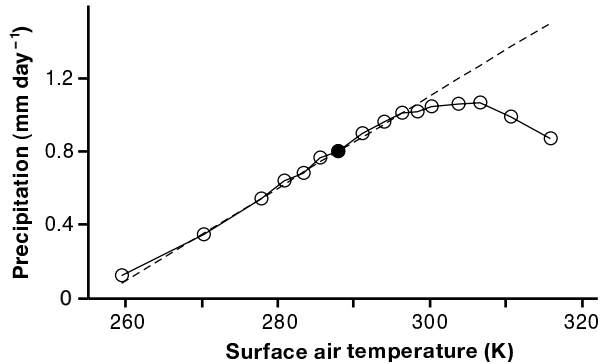


Figure 3. Global-mean large-scale precipitation (solid line and circles) vs global-mean surface air temperature. The dashed line represents a linear increase of $3.2\% \text{ K}^{-1}$ relative to the reference simulation. (From *O’Gorman and Schneider* [2007b].)

Figure 3 shows the large-scale precipitation as a function of global-mean surface air temperature. Like the total precipitation in Fig. 2, the large-scale precipitation increases approximately linearly with surface air temperature over a wide range of climates, with a similar fractional rate of increase relative to the reference simulation as the total precipitation. But unlike the total precipitation, the large-scale precipitation does not increase monotonically with surface air temperature but has a maximum in a moderately warm climate.

Changes in the thermal structure of the atmosphere and in characteristics of large-scale eddies are responsible for the changes in large-scale precipitation. Given the thermal structure of the atmosphere and eddy characteristics, a stochastic model of isentropic moisture advection and condensation (*O’Gorman and Schneider* [2006]) successfully accounts for the changes in large-scale precipitation. According to the stochastic model, the large-scale condensation rate depends on eddy kinetic energies and eddy length scales, on the merid-

ional gradient of saturation specific humidity along isentropes, and on the distance an air parcel travels along isentropes before it reaches saturation. Analyzing the stochastic model, we found the following factors to be important in accounting for the changes in large-scale precipitation: (i) As the climate warms, the slope of isentropes in the lower troposphere decreases. This reduces the meridional gradient of saturation specific humidity along isentropes relative to what it would be if only the saturation specific humidity would increase, leading to a relative reduction in the large-scale condensation rate. (ii) As the climate warms, the distance an air parcel travels to reach saturation increases in the lower troposphere, and it generally (except for the warmest climates) decreases in the upper troposphere. This, along with changes in the atmospheric thermal structure, implies an upward movement of the region in which the bulk of the large-scale condensation occurs to colder and dryer regions of the atmosphere, leading to modifications of the large-scale condensation rate. The region in which the bulk of the large-scale condensation occurs also moves meridionally, further modifying the large-scale condensation rate. (iii) Eddy kinetic energies have a maximum for a climate close to the reference simulation (*O’Gorman and Schneider* [2007a]) and are smaller for much colder and much warmer climates. This affects the transport of water vapor along isentropes and likewise modifies the large-scale condensation rate. See *O’Gorman and Schneider* [2007b] for details.

The behavior of the large-scale precipitation illustrates that energetic considerations alone do not suffice to account for precipitation changes. Changes in the thermal structure of the atmosphere and in eddy characteristics must also be taken into account. These lead to the mean large-scale precipitation not scaling with precipitable water and even lead to non-monotonic behavior of large-scale precipitation as a function of surface air temperature.

4. Precipitation extremes

The frequency of occurrence of different precipitation rates and its changes with climate in simulations with current climate models depend on poorly constrained specifics of convective parameterizations. For example, quasi-equilibrium convection schemes in which convective available potential energy (CAPE) is released at the rate at which it is produced by resolved motions prevent the build-up and intermittent release of CAPE and thus may underestimate the frequency of intense precipitation events. While they may simulate mean precipitation correctly, they may do so with a bias toward more frequent low-intensity precipitation events than would

occur in nature. Conversely, convection schemes with an overly stiff trigger or high thresholds for the occurrence of deep convection may have a bias toward more frequent high-intensity precipitation events than would occur in nature. Comparing observational data and climate simulations with different convection schemes, *Dai et al.* [1999], *Sun et al.* [2005], and *Wilcox and Donner* [2007], among others, did indeed find such biases in simulated precipitation statistics. *Wilcox and Donner* [2007] found that changes in the exceedance probability of a precipitation threshold are greater with changes in the convection scheme than with a 2-K surface warming with fixed convection scheme. Such findings cast doubt on the ability of current climate models and of our idealized GCM to simulate changes in precipitation extremes reliably.

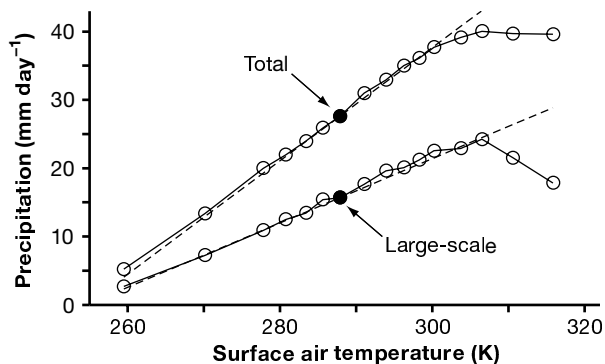


Figure 4. 99th percentiles of daily total and large-scale precipitation (solid lines and circles) vs global-mean surface air temperature. The two dashed lines represent linear increases of $3\% \text{ K}^{-1}$ relative to the 99th percentiles of total and large-scale precipitation in the reference simulation.

Here we present changes in precipitation extremes in our simulations, without any claim to universality of the results but to illustrate the complexity of possible changes in the extremes. Figure 4 shows the 99th percentiles of daily precipitation as a function of global-mean surface air temperature, both for total and large-scale precipitation. The 99th percentile is the amount of daily precipitation exceeded with probability 1% in precipitation events in model grid boxes. Over a wide range of climates, the 99th percentiles increase approximately linearly with surface air temperature, with a fractional rate of increase of about $3\% \text{ K}^{-1}$ relative to their values in the reference simulation. This fractional rate of increase is similar to that of the respective mean precipitations (Figs. 2 and 3) and is considerably smaller than that of precipitable water (Fig. 1). In warm climates, the 99th percentiles approach a maximum. They decrease slightly (for total precipitation) or more significantly (for large-scale precipitation) in yet warmer

climates.

The behavior of the 99th percentile of daily precipitation is similar to that of other high percentiles. Both for total and large-scale daily precipitation, high percentiles generally exhibit a linear regime with the same fractional rate of increase with surface air temperature of about $3\% \text{ K}^{-1}$. For very high percentiles (greater than about the 99.9th), the linear regime extends over the entire range of climates we simulated; there are no maxima in the percentiles. For moderately high percentiles (less than about the 97.5th), the maxima are more pronounced, and also the total precipitation percentiles exhibit a clear maximum in warm climates and decrease significantly in yet warmer climates.

It is unclear at present to what extent these results depend on the structure of the convection scheme in our GCM—an idealized quasi-equilibrium scheme (*Frierson* [2007])—and on parameters in the scheme. Additionally, the values of the percentiles and possibly also their fractional rates of change may be resolution dependent. In that high percentiles of daily precipitation in the vicinity of the Earth-like reference simulation exhibit a fractional rate of change with surface air temperature similar to that of the mean precipitation, our simulations differ from the comprehensive GCM simulations of *Kharin and Zwiers* [2005], who found a fractional rate of change of precipitation extremes with surface air temperature that exceeds that of the mean precipitation.¹ It is important to elucidate the reasons for such differences to gain confidence in simulations of changes in precipitation extremes.

What our results do show is that there is no general principle that would dictate that changes in precipitation extremes scale with changes in precipitable water. It is sometimes claimed that because large-scale and long-term energetic and dynamic balances do not constrain individual (local and transient) intense precipitation events, and because the water precipitating in intense precipitation events is primarily advected from other regions of the atmosphere, rather than being evaporated locally, changes in precipitation extremes may scale with changes in precipitable water (e.g., *Trenberth* [1999]; *Allen and Ingram* [2002]; *Hegerl et al.* [2007]). Our results show that this argument is not generally valid, apparently because it ignores that moisture convergence and precipitation in individual storms are directly linked to upward mass flux and latent heat release, which themselves must satisfy dynamic and thermodynamic balances (e.g., *Pauluis and Held* [2002a, b]).

¹Because, obviously, high percentiles of precipitation are greater than the respective mean values, the absolute rates of change in the percentiles are greater than those in the mean values when the fractional rates of change are equal.

The dynamics and thermodynamics of storms must play a central role in determining precipitation extremes and their changes with climate.

Acknowledgments. The research on which this report is based was supported by the National Science Foundation (Grant ATM-0450059) and by a David and Lucile Packard Fellowship. The numerical simulations were performed on Caltech’s Division of Geological and Planetary Sciences Dell cluster.

References

- Allen, M. R., and W. J. Ingram (2002), Constraints on future changes in climate and the hydrologic cycle, *Nature*, *419*, 224–232.
- Dai, A., F. Giorgi, and K. E. Trenberth (1999), Observed and model-simulated diurnal cycles of precipitation over the contiguous United States, *J. Geophys. Res.*, *104*, 6377–6402.
- Frierson, D. M. W. (2007), The dynamics of idealized convection schemes and their effect on the zonally averaged tropical circulation, *J. Atmos. Sci.*, *64*, 1959–1976.
- Hegerl, G. C., F. W. Zwiers, P. Braconnot, N. P. Gillett, Y. Luo, J. A. M. Orsini, N. Nicholls, J. E. Penner, and P. Stott (2007), Understanding and attributing climate change, in *Climate Change 2007: The Physical Science Basis. Contribution of Working Group I to the Fourth Assessment Report of the Intergovernmental Panel on Climate Change*, edited by S. Solomon, D. Qin, M. Manning, Z. Chen, M. Marquis, K. Averyt, M. Tignor, and H. Miller, pp. 664–745, Cambridge Univ. Press, Cambridge, UK, and New York, NY, USA.
- Held, I. M., and B. J. Soden (2000), Water vapor feedback and global warming, *Annu. Rev. Energy Environ.*, *25*, 441–475.
- Held, I. M., and B. J. Soden (2006), Robust responses of the hydrological cycle to global warming, *J. Climate*, *19*, 5686–5699.
- Khariin, V. V., and F. W. Zwiers (2005), Estimating extremes in transient climate change simulations, *J. Climate*, *18*, 1156–1173.
- Kiehl, J. T., and K. E. Trenberth (1997), Earth’s annual global mean energy budget, *Bull. Amer. Meteor. Soc.*, *78*, 197–208.
- O’Gorman, P. A., and T. Schneider (2006), Stochastic models for the kinematics of moisture transport and condensation in homogeneous turbulent flows, *J. Atmos. Sci.*, *63*, 2992–3005.
- O’Gorman, P. A., and T. Schneider (2007a), Energy of midlatitude transient eddies in idealized simulations of changed climates, *J. Climate*, submitted. Available at www.gps.caltech.edu/~tapio/papers/.
- O’Gorman, P. A., and T. Schneider (2007b), The hydrological cycle over a wide range of climates simulated with an idealized GCM, *J. Climate*, submitted. Available at www.gps.caltech.edu/~tapio/papers/.
- Pauluis, O., and I. M. Held (2002a), Entropy budget of an atmosphere in radiative-convective equilibrium. Part I: Maximum work and frictional dissipation, *J. Atmos. Sci.*, *59*, 125–139.
- Pauluis, O., and I. M. Held (2002b), Entropy budget of an atmosphere in radiative-convective equilibrium. Part II: Latent heat transport and moist processes, *J. Atmos. Sci.*, *59*, 140–149.
- Peixoto, J. P., and A. H. Oort (1992), *Physics of Climate*, 520 pp., American Institute of Physics.
- Sun, Y., S. Solomon, A. Dai, and R. W. Portmann (2005), How often does it rain?, *J. Climate*, *19*, 916–934.
- Trenberth, K. E. (1999), Conceptual framework for changes of extremes of the hydrological cycle with climate change, *Climatic Change*, *42*, 327–339.
- Trenberth, K. E., A. Dai, R. M. Rasmussen, and D. B. Parsons (2003), The changing character of precipitation, *Bull. Amer. Meteor. Soc.*, *84*, 1205–1217.
- Wilcox, E. M., and L. J. Donner (2007), The frequency of extreme rain events in satellite rain-rate estimates and an atmospheric general circulation model, *J. Climate*, *20*, 53–69.

T. Schneider and P. A. O’Gorman, California Institute of Technology, Pasadena, CA 91125, (e-mail: tapio@caltech.edu, pog@caltech.edu)

This preprint was prepared with AGU’s L^AT_EX macros v4, with the extension package ‘AGU++’ by P. W. Daly, version 1.6a from 1999/05/21.